Proposal of a model based fault identification neural technique for more-electric aircraft flight control EM actuators

Proposal of a model based fault identification neural technique for more-electric aircraft flight control EM actuators

MATTEO DALLA VEDOVA, PAOLO MAGGIORE, LORENZO PACE, SIMONE ROMEO
Department of Mechanical and Aerospace Engineering (DIMEAS)
Politecnico di Torino
Corso Duca degli Abruzzi, 24 - 10129 - Torino
ITALY
matteo.dallavedova@polito.it, paolo.maggiore@polito.it, lorenzo.pace@polito.it

Abstract: - There are many different ways to detect incipient failures of electromechanical actuators (EMA) of primary flight command provoked by progressive wear. With the development of a prognostic algorithm it's possible to identify the precursors of an electromechanical actuator failure, to gain an early alert and so get a proper maintenance and a servomechanism replacement. The present work aims to go beyond prognostic algorithms strictly technology-oriented and based on accurate analysis of the cause and effect relationships because if on one hand they show great effectiveness for some specific applications, instead they mostly fail for different applications and technologies. Through the development of a simulation test bench the authors have demonstrated a robust method to early identify incoming failures and reduce the possibility of false alarms or non-predicted problems. Authors took into account friction, backlash, coil short circuit and rotor static eccentricity failures and defined a model-based fault detection neural technique to assess data gained through Fast Fourier Transform (FFT) analysis of the components under normal stress conditions.

Key-Words: - Artificial Neural Network (ANN), Electromechanical Actuator (EMA), BLDC Motor Failures, Fault Detection/Identification Algorithm, Prognostics

1 Introduction

In Aeronautics there are many components characterized by limited life duration even though conceived to last much more than the maintenance interval foreseen (*safe life* approach). Many elements can occur to provoke a reduction of such duration (i.e. unmonitored loads) and a malfunction can cause the inability to perform functionalities at the desired level. The *safe life* approach has got some limits because, as it doesn't consist in the evaluation of the real status of the components, maintenance is restricted to the specific scheduled operations. As a matter of fact, potential initial flaws, possibly deriving from the manufacturing process, could degenerate in a sudden fault compromising the aircraft safety. Moreover, the *safe-life* criterion does not allow the individuation of the cause and the location of the malfunctioning while, as the replacement of the single failed component could be sufficient to restore the system functionality, its accurate identification could permit to replace it and not the whole system. As a consequence, this kind of intervention would entail a higher efficiency and a reduction of costs of the maintenance process.

In recent years, prognostic concepts, because of their applications and strong impact, have attracted the attention of a large part of the scientific and technological community with reflection on the scientific literature. Despite contributions are often innovative and meaningful, they tend to disregard a comprehensive approach (i.e. systemic vision), being too theoretical or specific.

The purpose of the prognostic is to extend the functionality and the efficiency for the desired performances of a component and to avoid unexpected failures able to threaten the mission of the system. In order to obtain such results, all possible failure modes have to be scouted and the ability to individuate the first symptoms of aging or wear has to be improved. A database of possible behaviors has to be settled, filled and planned in order to be effectively used for a proper failure propagation model.

The Prognostics and Health Management (PHM) provides real-time data of the current status of the system and calculates the Remaining Useful Life (RUL) before a fault occurs; in fact, it analyzes the behavior of components and determines if they are damaged and need maintenance.

This approach represents an asset in comparison with the results obtained with classical monitoring and maintenance concepts (e.g. based on overhaul or life-limited parts) and it brings along many benefits such as: diminished operating costs, less maintenance interventions required, reduced amount of necessary redundancies, improved aircraft safety and reliability, simplified logistic. On the base of these analysis, maintenance actions can be planned appropriately and, as a consequence, downtime and related costs are limited and the management of spare parts warehouses is more effective.

In this paper, the authors propose a more systemic and multidisciplinary approach: the electrical and mechanical characteristics of the actuator and its relevant failure modes are analyzed and modeled together in a multi-domain numerical mode implemented in MATLAB Simulink® simulation environment. The present research is focused on a fault detection/evaluation technique able to identify the failure precursors and evaluate the corresponding damage entity; the model aims to analyze the EMA performance and the effects of different progressive faults. We used the numerical analysis of the Fast Fourier Transform of the closed loop signals to identify proper precursors of the considered faults that an innovative neural prognostic algorithm can successfully reveal and properly identify. In order to assess the actual ability of the algorithms to correctly sort out the failure precursors, we developed a simulation test bench based on the injection of an irregular degradation pattern into the flight control system. This method seems affordable for the early identification of malfunctioning, because it reduces the risk of false alarms or unrevealed failures. To ensure the feasibility of the application of the proposed prognostic method on aircraft in the civil aviation category, real-time inflight analysis is not implemented because it refers only to preflight / postflight or ordinary maintenance procedures, when the data can be analyzed by an external computer without affecting the normal inflight operations. Furthermore, the proposed algorithms don't introduce additional components or new sensors because they use only information got from transducers derived from virtual sensors that post-process actual raw measurements or from the ones that already equip the considered system. These algorithms can be easily integrated in an automatic check process system, which can be performed by the maintenance staff. The built-in test can be executed without the component disassembly and requires a simple postprocessing and analysis of the downloaded data.

2 Primary Flight Control EMA

Primary flight controls are conceived to adjust and control the aircraft flight dynamic: thorough the rotation of the corresponding aerodynamic surfaces they generate unbalanced forces/couples acting on the aircraft. These controls usually make the aircraft rotate around one of the three body axis when one control surface is activated, possibly minimizing the coupling effects. In particular, aircraft primary flight controls are typically proportional servomechanisms with continuous activation: they must return a force feedback related to command intensity and a high frequency response. As their loss is a critical issue, their reliability must be very high. Until a few years ago, in aeronautical applications were employed hydromechanical and then, with the introduction of fly-by-wire technology, electrohydraulic actuators. Thanks to their high specific power and very high reliability, current aircrafts are often equipped with them. However, in more modern airliners are installed electro-hydrostatic (EHA) or electro-mechanical actuators (EMA).

The Electro-Hydrostatic actuator (EHA) usually consists of an electrical motor that converts electrical power into mechanical power, then transformed into hydraulic power through an axial piston pump. It replaces the hydraulic line with an electric signal and the highly-pressurized hydraulic fluid is maintained only near the actuator. This allows a consistent weight reduction. Moreover, according to the architecture, it can be employed a linear or rotary actuator. For all these reasons, EHAs provide attractive benefits and represent an interesting alternative to traditional hydraulic controls.

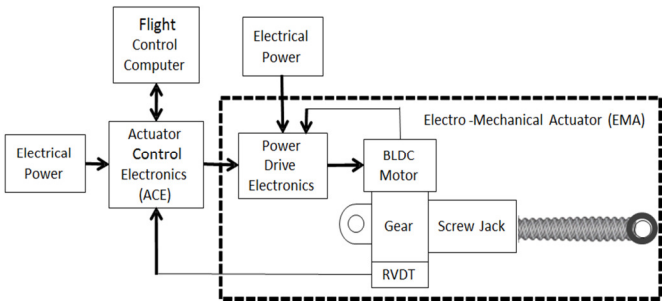

Fig. 1: Electromechanical actuator (EMA) scheme

Nevertheless, in the last years, the trend moved towards all-electric aircrafts and towards an extensive application of novel optimized electrical actuators, such as the electromechanical ones (EMA). In this field, the scientific activity is fervent and the interest of the aeronautical world is very high because, compared to the electrohydraulic actuators, the EMAs offer many advantages.

In particular, it must be noted that overall weight is reduced, maintenance is simplified and hydraulic fluids, often contaminant, flammable or polluting, can be eliminated. As a matter of fact, as reported in [1], the use of actuation systems based on EMAs has been increasing in various fields of the aerospace technology.

As shown in Fig.1, a typical EMA actuator used in a primary flight control is composed by:

1. an actuator control electronics (ACE) that closes the feedback loop comparing the commanded position (FBW) with the actual one and gives the reference current I_{ref};
2. a power drive electronics (PDE) that regulates the three-phase electrical power;
3. an electrical motor, often BLDC type;
4. a gear reducer having the function to decrease the motor angular speed (RPM) and increase its torque to desired values;
5. a system that transforms rotary motion into linear motion (e.g. ball-screws or roller-screws);
6. a network of sensors used to close the feedback rings (current, angular speed and position) that control the whole actuation system (RVDT).

3 EMA Numerical Model

As previously mentioned, goal of this research is the proposal of a new technique able to identify precocious symptoms (usually defined as failure precursors) of EMA degradations.

In order to assess the feasibility, the performance and the robustness of the aforesaid technique, a suitable simulation test bench has been developed in MATLAB/Simulink®. This numerical model, that is widely described in [2], is coherent with the considered EMA architecture shown in Fig. 1.

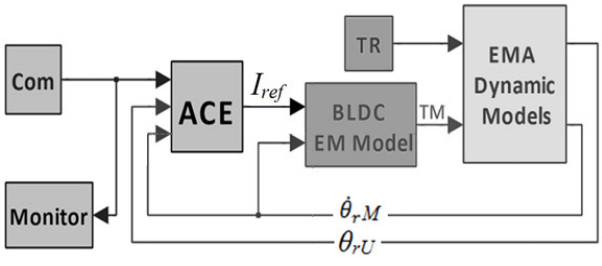

Fig. 2: Proposed EMA block diagram

As shown in Fig. 2, the propose EMA simulation model is composed by six different subsystems:

1. *Com*: input block that generates the different position commands.
2. *ACE*: subsystem simulating the actuator control electronics, closing the feedback loops and generating as output the reference current I_{ref}.
3. *BLDC EM Model*: subsystem simulating the power drive electronics and the trapezoidal BLDC electromagnetic model, that evaluates the torque developed by the electrical motor as a function of the voltages generated by a three-phase electrical regulator.
4. *EMA Dynamic Model*: subsystem simulating the EMA mechanical behavior by means of a 2 degree-of-freedom (d.o.f.) dynamic system.
5. *TR*: input block simulating the aerodynamic torques acting on the moving surface controlled by the actuator.
6. *Monitor*: subsystem simulating the EMA monitoring system.

It must be noted that this numerical model is able to simulate the dynamic behavior of the considered EMA servomechanism taking also into account the effects of BLDC motor non-linearities [3-7], end-of-travels, compliance and backlashes acting on the mechanical transmission [8], analogic to digital conversion of the feedback signals, electrical noise acting on the signal lines and electrical offset of the position transducers [9] and dry friction (e.g. acting on bearings, gears, hinges and screw actuators) [10].

4 Considered EMA Progressive Faults

As EMA have been only recently employed in aeronautics, their cumulated flight hours are still not enough to provide reliable statistics data about more recurring failures. However, it is possible to single out four main failure categories: mechanical or structural failures, BLDC motor failures, electronics failures and sensor failures.

The present work has been mainly focused on the effects of mechanical failures due to progressive wear, which causes an increase of backlash and friction, and on two typical BLDC motor failures: the coil short-circuits (SC) and the bearing wear generating rotor static eccentricity (RE).

As a general rule, the detection/evaluation of mechanical failure due to friction or backlash is usually directly performed by analyzing specific characteristics of the dynamic response of the system (e.g. position, speed or acceleration).

Vice versa, in case of motor progressive failures, such as SC or RE, the characteristics of the mechanical transmission, in terms of inertia, dry and viscous frictions, backlashes, noises, etc., could disguise or mitigate the failure effects making inaccurate, if not ineffective, any prognostic effort. In these cases the analysis of electrical harmonics (e.g. phase currents) provides a better understanding of the failure progression and its estimation is far more accurate.

Electrical and sensor failures are not less important than the others, but their evolutions are usually very fast, if not instantaneous, and the corresponding precursors are often difficult to identify and evaluate in order to perform the fault detection/identification.

The mechanical wear can also generate backlash in EMA moving parts such as gears, hinges, bearings and especially screw actuators. These backlashes, acting on the mechanical elements of the transmission, reduce the EMA accuracy and can lead to problems of reduced stiffness and reduced controllability of the whole actuator [10].

The most important progressive faults affecting BLDC motors can be generated by short-circuits of the stator coils or by wear phenomenon affecting the rotor bearing (generating a rotor static eccentricity).

Short-circuit fault can actually occur within a coil, between two coils of the same phase, and between two different phases: given that the first case is the most common and generally occurs first, only the first case is considered in this paper. According to [11], it is also assumed that each phase winding consists of turns connected in series and the three-phase windings are wye-connected with a floating neutral point.

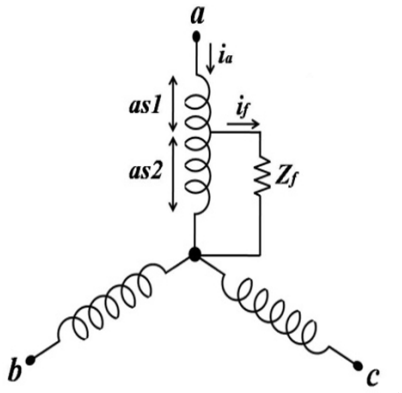

Fig. 3: Schematic of turn-to-turn coil short circuit [11].

A schematic of the three-phase windings with an inter-turn fault in the *a*-phase winding is shown in Fig. 3, where *as1* and *as2* represent the healthy and the shorted turns, respectively, i_a is the *a*-phase current, i_f is the circulating current in the shorted turns and Z_f represents the possible external impedance between the shorted turns [12].

It must be noted that stator short-circuits usually start between a few turns belonging to the same phase coil (turn-to-turn coil short circuit failure). As in short-circuited coils the voltage remains the same and the resistance decreases, the resulting current increases, generating a localized temperature rising in the conductor that, degrading the insulating paint, favors the extension of the failure to adjacent coils.

If this kind of fault is not promptly detected it could propagate and generate severe phase-phase or phase-neutral BLDC motor failures.

The static eccentricity of a rotating body consists in a misalignment between the rotor rotation axis and the stator axis of symmetry. This misalignment is mainly due to tolerances and imperfections introduced during motor construction or to a gradual increase of wear of the rotor shaft bearings. When this failure occurs, the motor having more than one polar couple generates a periodically variable magnetic flux, as the air gap varies during its angular rotation. In case of static eccentricity, the air gap changes during the rotor spinning (Fig. 4) as a function of the rotor position θ_r:

$$g'(\theta_r) = g_0 + x_0\cos(\theta_r) \tag{1}$$

where g_0, is the clearance between stator and rotor, without considering misalignments, and the second term represents the variation of the air gap. In terms of motor performances, as reported in [13], the provided torque is lower than in nominal conditions, whereas, spectral analysis reveals the presence of sub-harmonics increasing for higher eccentricities.

The rotor static eccentricity and the partial stator coil short circuit effects have been modeled by means of a simplified numerical algorithm.

As both the failures change the magnetic coupling between stator and rotor, in fact, failures can be modelled by modifying the values and angular modulations of the back-EMF coefficients:

$$ke_a = ke_a \cdot Ce_a \cdot (1 + \zeta\cos(\theta_r)) \tag{2}$$

where ζ is the rotor static eccentricity.
The constants ke_a, ke_b and ke_c are then used to calculate the corresponding counter-electromotive forces, e_a, e_b and e_c, and to evaluate the mechanical couples, Ce_a, Ce_b and Ce_c, generated by the three motor phases. The effects that these progressive failures produce on the dynamic behaviors of the considered actuation system are discussed in [2].

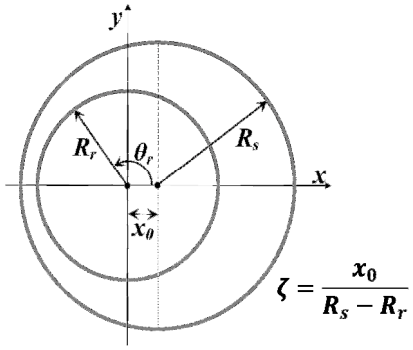

Fig. 4: BLDC Motor Rotor static eccentricity ζ: schematic of the reference system

5 Proposed FDI Algorithm

As previously reported, an innovative model based fault detection and identification (FDI) technique, based on neural identification, is proposed as a prognostic method which analyzes data obtained through FFT spectral analysis [14-17]. In order to overcome the shortcomings found in the FDI algorithm proposed in [1], the authors developed an enhanced method, schematically reported in Fig. 5, based on two distinct checks:

1. the first step of the FDI algorithm is based upon a simple deterministic algorithm that performs the fault detection (acting a simple selection between healthy and faulty system) as a function of the maximum value of the phase currents;
2. the second one is realized by means of two Multilayer Perceptron (MLP) Neural Networks (NNs), each one designed and trained to perform a specific task [18]: the first neural network (ANN1) detects the damage type and classify it according to a predefined classification scheme, whereas the second network (composed by two parallel neural networks ANN2_SC and ANN2_RE, each specialized to evaluate a single type of progressive fault) provides a measure of the corresponding fault magnitude, according to a quantification scheme.

The FDI method is performed analyzing the dynamic response of the EMA in case of high amplitude step position command *Com*, evaluating the evolution of defined physical parameters (e.g. the time-history of the here phase currents and the actuation speed) and extrapolating the information necessary to the NNs to process the aforesaid classification. In particular, the values of speed and currents are recorded in two matrices, referring to growing fault level conditions, where the magnitude of the considered faults can vary within proper ranges. Furthermore, proper levels of random noise are added to these signals (simulating experimental measures) in order to evaluate the robustness of the proposed method.

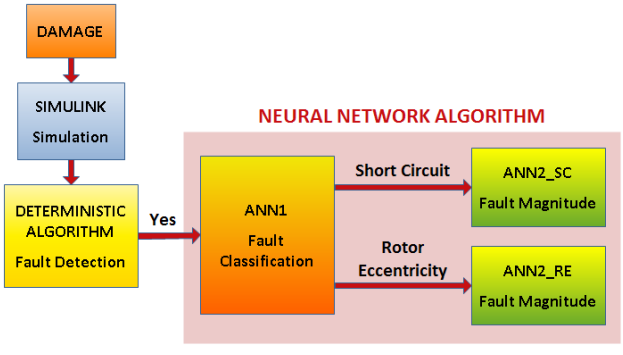

Fig. 5: Schematic of the proposed FDI algorithm

5.1 Maximum Phase Current Analysis

Analyzing the correlations between the progressive faults and the corresponding BLDC phase currents, the authors found that the peak value of the three phase currents highlights a strictly monotone growing trend that is common to the different types of failure considered. Given that the maximum value of the phase current i_{max}, net of disturbances due to line noise and ripple to the switching of the inverter, do not exhibit significant drifts when the system operates in nominal conditions, the authors developed an algorithm capable of discriminating the state of the system and, if necessary, declare the incipient fault condition when the said value of peak current exceeds an appropriate reference band.

Fig. 6: Effect of the considered faults (% of Re or SC) on the maximum value of the phase current i_{max}

5.2 DataAnalysis: Phase Current

The signal features, derived as a consequence of a defined fault condition, have been identified, evaluated and mathematically defined.

Comparing each other Fig. 7 and Fig. 8, related to two different fault conditions, it is possible to define a correlation between these faults (types and magnitudes) and the distribution of the concavity of the phase current signals, in correspondence of the Two-Phase ON (TPO) phenomena.

By approximating this part of the signal with a second degree equation and by varying the extent of the fault, it is observed that, in conditions of static rotor eccentricity (RE), for each phase, concavity is always positive, while short-circuit (SC) faults put in evidence an alternation of the signs of the concavity: two negatives and one positive in the TPO positive portion and vice versa, two positives and one negative when the TPO is the negative.

Analyzing all the positive and negative TPO sections as a single signal, it is possible to remark another observation regarding the signal symmetry: the SC fault condition shows symmetry with respect to the horizontal axis of the positive and negative signals (Fig. 7), while the RE condition shows a simply shifting of the aforesaid signal (Fig. 8).

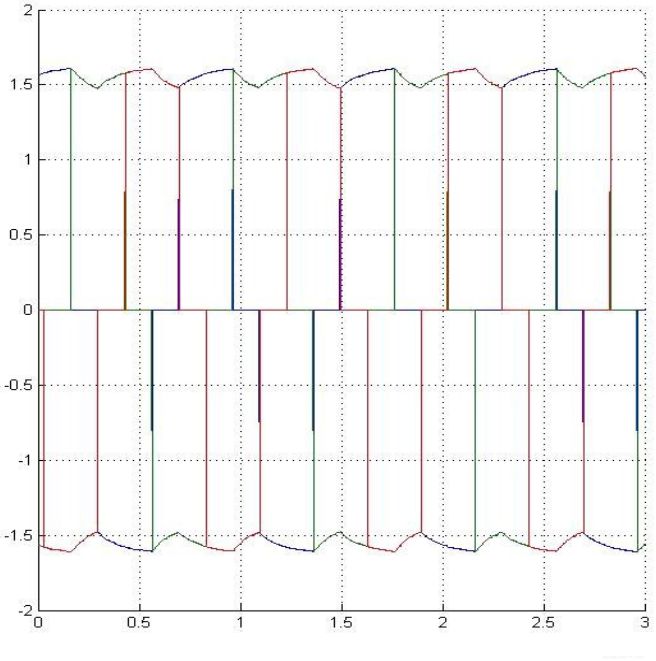

Fig. 7: Reference current - 25% short-circuit (SC)

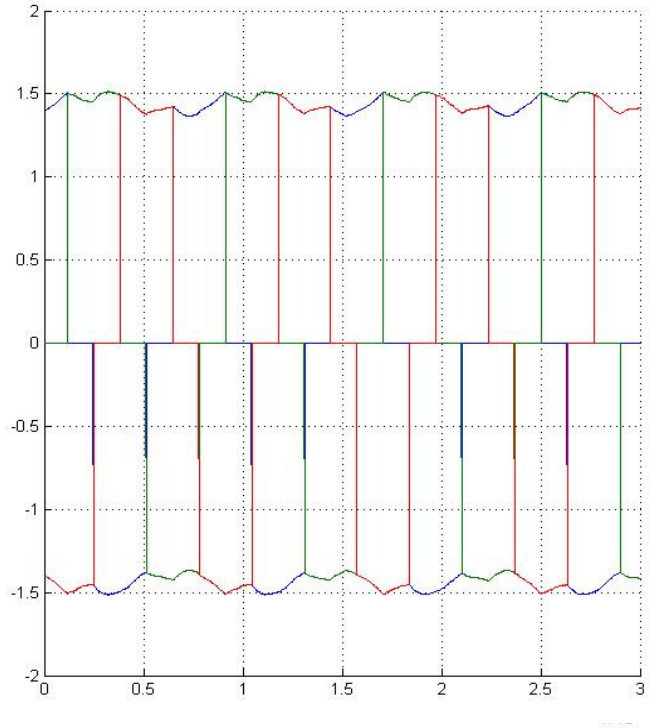

Fig. 8: Reference Current - 5% rotor eccentricity (RE)

5.3 Data Analysis: Speed

The behavior of the phase currents under fault conditions influences the behavior of the rotor speed. Through proper FFT analysis is possible to observe characteristic frequencies changing their magnitude when the failure increase: frequencies around the values of 0 Hz, 251 Hz, 503 Hz and 755 Hz are peculiar of the SC fault, whereas the RE fault features frequencies around the values of 0 Hz, 122 Hz, and 375 Hz. Also in this case maximum, minimum and average value trends are important to evaluate.

5.4 FDI Neural Network

The fault identification function (classification of the progressive fault type and evaluation of its magnitude) is performed by means of two neural networks, respectively called ANN1 and ANN2_SC or ANN2_RE, previously described in [1].

The first neural network (i.e. ANN1), that is activated when the *Maximum Phase Current* algorithm (shown in paragraph 5.1) identifies an eventual faulty condition, has to perform a first classification of the detected fault, discriminating a given condition of system failure through the considered single-fault conditions (i.e. SC and RE).

The network is trained to associate a training vector P, elaborated from the MATLAB/Simulink® data, to a target vector T_{ANN1}. The training set P is composed of 126 rows, divided in 3 sections, each one characterized by a different noise level. Every section (42 rows each) contains two types of faulty data: a first half coming from SC faults and a second half coming from RE conditions.

Each row of the aforesaid training vector P is structured with 7 characteristic elements:

- three concavities: by means of the values +1 or -1, those elements represent the three positive PhaseON concavities;
- two velocity frequencies: the two main carrier frequencies of velocity;
- two current parameters: the mean and maximum values of the envelope signal of the three PhaseON.

The vector target T_{ANN1} consists of three equal sections of 42 rows each for 2 columns: SC faults are represented by a unitary value in the first column, while at the contrary the RE faults have a unitary value in the second column (Fig. 9).

The ANN1 is a pattern recognition neural network and is shaped as a single-hidden-layer perceptron, with a Log-Sigmoid activation function on the hidden layer.

$$T_{ANN1} = \begin{bmatrix} 1 & 0 \\ 1 & 0 \\ 1 & 0 \\ 0 & 1 \\ 0 & 1 \\ 0 & 1 \end{bmatrix} \begin{matrix} \} \text{SC fault} \\ \\ \\ \} \text{RE fault} \\ \\ \end{matrix}$$

Fig. 9: ANN1 target vector

The task of the second neural network (i.e. ANN2) is to provide a quantification of the failure extent. Given that the two considered faults have a different evolution, and in order to achieve a more precise evaluation of these fault level, this NN is splitted in two different neural networks (ANN2_SC and ANN2_RE), each one specialized in a single type of fault. According to the type of progressive fault detected by the first network ANN1, only one of these ANN2s is activated.

The training vectors *P* of the two ANN2 have the same macro-structure of the ANN1 training vector, with 3 sections characterized by a different noise level. As for the ANN1, also the two ANN2 neural networks perform a pattern recognition task; they are characterized to an identical morphology, but have different dimensions, due to an optimization procedure.

The ANN2_SC training vector *P* contains 11 elements in each row:

- four velocity FFT magnitudes: those elements indicate the amplitudes of the four characteristic peaks of the FFT speed signal (frequency: 0 Hz, 251 Hz, 503 Hz and 755 Hz);
- two current parameters: the mean and maximum values of the envelope signal of the three PhaseON;
- five current FFT magnitudes: those elements represent the first five peaks of the current FFT.

The ANN2_RE training vector contains 12 elements in each row:

- four velocity FFT magnitudes: those elements indicate the amplitudes of the four characteristic peaks of the FFT speed signal (frequency: 0 Hz, 122 Hz and 375 Hz);
- two velocity parameters: those elements relate to the relationship between the maximum value and the minimum value of the speed signal, and between the maximum value and the mean value of the speed signal;
- two current parameters: the mean and maximum values of the envelope signal of the three PhaseON,
- five current FFT magnitudes: those elements represent the first five peaks of the current FFT.

For instance, assuming a classification pattern characterized by three levels of failure, the corresponding target vector T_{ANN2} , as shown in Fig. 10, results composed of three columns representing respectively small, medium and large fault conditions[1]. Also in this case a unitary value in a row permits the detection of the right fault.

$$T_{ANN2} = \begin{bmatrix} 1 & 0 & 0 \\ 1 & 0 & 0 \\ 1 & 1 & 0 \\ 0 & 1 & 0 \\ 0 & 1 & 1 \\ 0 & 0 & 1 \\ 0 & 0 & 1 \end{bmatrix} \begin{matrix} \} \text{Small fault level} \\ \\ \} \text{Medium fault level} \\ \\ \} \text{Large fault level} \end{matrix} \begin{matrix} \\ \\ \leftarrow \underline{\text{INTERSECTION}} \\ \\ \leftarrow \underline{\text{INTERSECTION}} \\ \\ \\ \end{matrix}$$

Fig. 10: ANN2 target vector

It must be noted that these target vectors don't present a net distinction from case to case (as it is for the T_{ANN1}) in their structure. In fact, the target vectors are structured with an element shared between two different contiguous fault level: these elements are called intersection and, introducing an overlap between adjacent levels, allow improve the fault detection capability of these NNs (see Fig. 10). It is observed that around the intersections there are bands of interference (i.e. range of fault percentages, typically from 2% up to 5%) in which both fault levels are perceived.

6 Results

Each Neural Network provides results in the form of percentage of probability that the input corresponds to the fault indicated by the target vector column. Those results are shown to the user as row vectors.

The ideal output of ANN1 to an SC input should be in the form Y = [1 0], whereas, in case of RE, the output should be Y = [0 1]. It must be noted that, as shown in Table 1 and Table 2, the real results are very close to the theoretical ones.

Table 1: SC fault recognition

Short-circuit fault	Y = sim (net, P_{tester})	
Fault entity	-	-
97%	0.9999	0.0001
91%	1	0
80%	1	0
70%	1	0

1 The entity of these fault levels will be specified in more detail in the following paragraph (Fig. 11 and 12).

Table 2: RE fault recognition

Rotor eccentricity fault	Y = sim (net, P_{tester})	
Fault entity	-	-
0,4%	0.0009	0.999
0,9%	0.0009	0.9991
1,8%	0.0009	0.999
3.2%	0.0009	0.9988

The results reported in Table 3 and Table 4 are relative to the two ANN2 conceived for a three levels classification. The ideal output should be Y = [1 0 0] for a small fault, Y = [0 1 0] for a medium fault and Y = [0 0 1] for a large fault, but in reality those results are more shaded.

Table 3: Results obtained by SC fault analysis

Fault	Small	Medium	Large
3,00%	0,9983	0,0137	0,0012
4,50%	0,9835	0,0814	0,0011
6,50%	0,7688	0,4712	0,0007
8,20%	0,0308	0,991	0,0008
9,70%	0,048	0,9962	0,0015
13,00%	0,0001	0,9998	0,0005
15,80%	0	0,9819	0,022
18,30%	0,0002	0,7244	0,5025
20,20%	0,0001	0,0684	0,959
22,60%	0	0,0122	0,9995

Table 4: Results obtained by RE fault analysis

Fault	Small	Medium	Large
4,7%	0,8714	0,3649	0,0007
6,1%	0,0366	0,9917	0,0049
8,9%	0,0025	0,9978	0,0225
10,1%	0,0047	0,9975	0,0091
14,5%	0,0006	0,999	0,0134
16,9%	0,0001	0,9985	0,0732
18,8%	0	0,999	0,7035
21,2%	0	0,9978	0,8311
24,6%	0	0,0095	0,9991
27,6%	0	0,0506	0,9972

Plotting those results (as shown in Fig. 11 and 12) it is possible to state the real behavior of the proposed algorithm (and its ability to perform the aforesaid classification) and it is also possible to evaluate the magnitude of the aforesaid bands of intersection caused by the overlapping of two contiguous fault levels in the target vector T_{ANN2}.

It should be noted that, from a technical point of view, nothing prevents to increase the fault levels to more than three. The analysis performed on more than four fault levels, though, show that the interference band widen to such an extent that the network detection capability is impaired.

This result represents only a theoretical limitation, however, as widening the level classification beyond a certain level would bring no real benefit to the prognostic analysis, with the only outcome of possible misinterpretation of result.

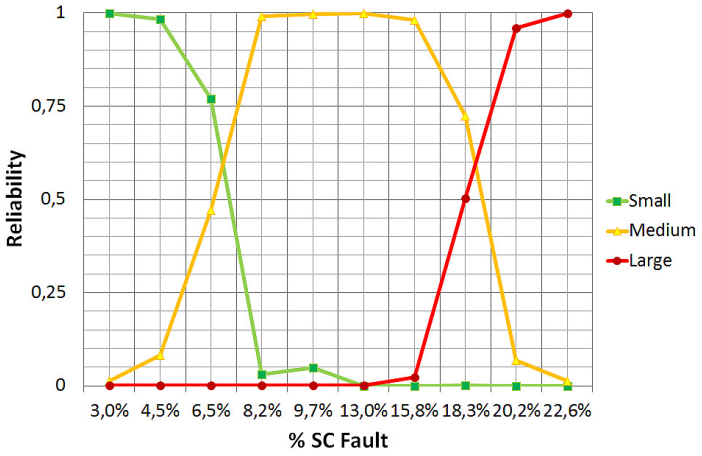

Fig. 11: ANN2_SC – results by SC fault analysis

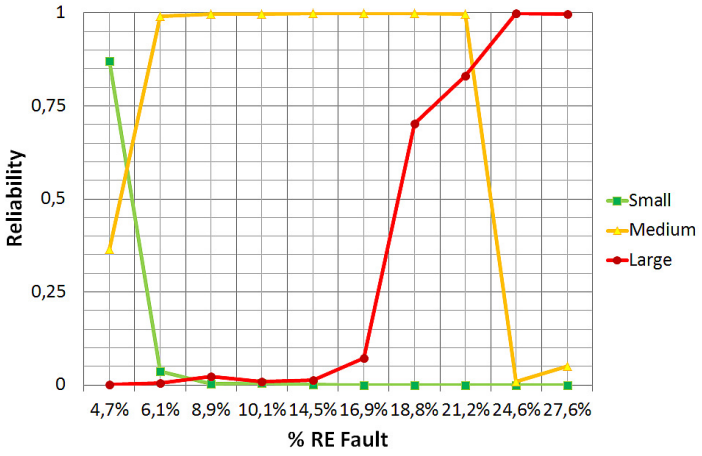

Fig. 12: ANN2_RE – results by RE fault analysis

7 Conclusions

The obtained preliminary results prove that the proposed prognostic technique is successful for the diagnosis of the state of a BLDC motor even if the neural networks employed are very simple and not yet optimized. In the present work, the authors analyzed two faults: short-circuit of a stator coil and static eccentricity of the rotor and we overlooked the cross effects. Nevertheless, the obtained results encourage the use of the proposed technique to focus the research on other challenging issues, such as the electrical and sensor failures, where the development of progressive faults is frequently very fast and the corresponding failure precursors are often difficult to identify and evaluate.

To this purpose, the actuator model should be further detailed and new elements should be modeled. Combined failures should also be investigated.

References:

[1] M. Battipede, M. D. L. Dalla Vedova, P. Maggiore, S. Romeo, Model based analysis of precursors of electromechanical servo mechanisms failures using an artificial neural network, *AIAA Modeling and Simulation Technologies Conference*, Kissimmee, Florida, 2015.

[2] P. Maggiore, M. D. L. Dalla Vedova, L. Pace, A Desando, Proposal of fault analysis parametric method applied to an electro mechanical servomechanisms affected by failures, International Journal of Prognostics and Health Management, Vol.6, No.1, 2015, ISSN: 2153-2648

[3] M. Çunkas, O. Aydoğdu, Realization of Fuzzy Logic Controlled Brushless DC Motor Drives using Matlab/Simulink, *Mathematical and Computational Applications*, Vol.15, 2010, pp. 218-229.

[4] A. Halvaei Niasar, H. Moghbelli, A. Vahedi, Modelling, Simulation and Implementation of Four-Switch Brushless DC Motor Drive Based On Switching Functions, *IEEE EUROCON 2009*, St. Petersburg, 2009, pp. 682 -687.

[5] B. K. Lee, M. Ehsani., Advanced Simulation Model for Brushless DC Motor Drives, *Electric Power Components and Systems*, Vol.31, No.9, 2003, pp. 841-868. ISSN: 1532-5008.

[6] T. Hemanand, T. Rajesh, Speed Control of Brushless DC Motor Drive Employing Hard Chopping PWM Technique Using DSP, *Proceedings of India International Conference on Power Electronics (IICPE 2006)*, 2006.

[7] T. A. Haskew, D. E. Schinstock, E. Waldrep, Two-Phase On' Drive Operation in a Permanent Magnet Synchronous Machine Electromechanical Actuator, *IEEE Trans. on Energy Conversion*, Vol.14, No.2, 1999.

[8] L. Borello; G. Villero, M. D. L. Dalla Vedova, New asymmetry monitoring techniques: effects on attitude control, *Aerospace Science and Technology*, Vol.13, No.8, 2009, pp. 475-487.

[9] L. Borello, M. D. L. Dalla Vedova, G. Jacazio, M. Sorli, A Prognostic Model for Electrohydraulic Servovalves, *Annual Conference of the Prognostics and Health Management Society*, San Diego, CA, 2009.

[10] L. Borello, and M. D. L. Dalla Vedova, A dry friction model and robust computational algorithm for reversible or irreversible motion transmission, *International Journal of Mechanics and Control*, Vol.13, No.2, 2012, pp. 37-4.

[11] B. W. Kim, K. T. Kim, J. Hur, Simplified impedance modeling and analysis for inter-turn fault of IPM-type BLDC motor, *Journal of Power Electronics*, Vol.12, 2012, pp. 10-18. ISSN: 1598-2092

[12] J. A. Farooq, A. Djerdir, A. Miraoui, Modelling and simulation of stator winding inter-turn faults in permanent magnet synchronous motors, *COMPEL - The International Journal for Computation and Mathematics in Electrical and Electronic Engineering*, Vol.27, No.4, pp. 887–896, 2008. ISSN: 0332-1649

[13] D. Belmonte, M. D. L. Dalla Vedova, P. Maggiore, New Prognostic Method Based on Spectral Analysis Techniques Dealing with Motor Static Eccentricity for Aerospace Electromechanical Actuators, *WSEAS Transactions On Systems*, Vol.14, 2015, pp. 45-53. ISSN: 1109-2777.

[14] P. D. Welch, The Use of Fast Fourier Transform for the Estimation of Power Spectra: A Method Based on Time Averaging Over Short, Modified Periodograms, *IEEE Transactions on audio and electroacoustics*, Vol.AU-15, No.2, 1967.

[15] A. Cardona, A. Lerusse, M. Géradin, Fast Fourier nonlinear vibration analysis, *Computational Mechanics*, Vol.22, No.2, 1998, pp. 128-142.

[16] W. Huaqing, C. Peng, Fault Diagnosis Method Based on Kurtosis Wave and Information Divergence for Rolling Element Bearings, *WSEAS Transactions on Systems*, Vol.8, No.10, October 2009, pp. 1155-1165.

[17] E. E Ngu, K. Ramar, R. Montano, V. Cooray, Fault characterisation and classification using wavelet and fast Fourier transforms, *WSEAS Transactions on Signal Processing*, Vol.4 No.7, July 2008, pp. 398-408.

[18] I. Chopra, R. Ganguli, D. J Haas, Detection of Helicopter Rotor System Simulated Faults Using Neural Networks, *Proceedings of the 37th Structures, Structural Dynamics and Materials Conference (AIAA-96-1646-CP)*, Salt Lake City, Utah, 15-17 April 1996, pp. 1246-1263.